Electronic Supplementary Material (ESI) for ChemComm.

X-Ray Excited Ultralong Room-Temperature Phosphorescence for Organic Afterglow Scintillator

Lele Tang, Jie Zan, Hao Peng, Xi Yan, Ye Tao,* Dan Tian, Qingqing Yang, Huanhuan Li, Qiushui Chen, Wei Huang,* Runfeng Chen*

L. Tang, H. Peng, X. Yan, Prof. Y. Tao, Q. Yang, Dr. H. Li, Prof. W. Huang, Prof. R. Chen
Key Laboratory for Organic Electronics and Information Displays & Jiangsu Key Laboratory for Biosensors, Institute of Advanced Materials (IAM), Nanjing University of Posts & Telecommunications, 9 Wenyuan Road, Nanjing 210023, China

J. Zan, Prof. Q. Chen
MOE key laboratory for analytical science of food safety and biology Institution, College of Chemistry, Fuzhou University, Fuzhou, 350108, China

Dr. D. Tian
College of Materials Science and Engineering, Co-Innovation Center of Efficient Processing and Utilization of Forest Resources, Nanjing Forestry University, Nanjing 210037, China

Prof. W. Huang
Frontiers Science Center for Flexible Electronics, Xi'an Institute of Flexible Electronics (IFE) and Xi'an Institute of Biomedical Materials & Engineering, Northwestern Polytechnical University, 127 West Youyi Road, Xi'an 710072, China.

Content

1. Synthesis and characterization

Materials: All reagents, unless otherwise specified, were purchased from Aldrich, Acros or Alfa Aesar, and used without further purification. Manipulations involving air-sensitive reagents were performed in an atmosphere of dry argon. Dichloromethane (DCM) was dried and purified by routine procedures.

Instruments: ^{1}H and ^{13}C-nuclear magnetic resonance (NMR) spectra were recorded on Bruker Ultra Shield Plus 400 MHz instruments with $CDCl_3$ as the solvents and tetramethylsilane (TMS) as the internal standard. High resolution mass spectra (HRMS) was collected by a Q-FT-MS on Bruker Solarix 7T instrument.

Pyridine-2,6-diylbis((9H-carbazol-9-yl)methanone) (DCzCOPy)

To a 50 mL double bottle charged with 9*H*-carbazole (Cz, 1.67 g, 10 mmol) and Sodium hydride (NaH) (0.6 g, 15 mmol) was injected 30 mL N, N-Dimethylformamide (DMF) using a syringe under an argon atmosphere at 25°C. The mixture was stirred at room temperature for 30 min. Subsequently, the resulting mixture was slowly added to a solution of pyridine-2,6-dicarbonyl dichloride (1.26 g, 5 mmol) in DMF (10 mL) at 25°C. [1] To complete the reaction, the reaction mixture was refluxed overnight. The reaction mixture was quenched by adding 10 mL water, and was extracted with DCM for three times (3×100 mL). The organic layer was collected and dried with anhydrous sodium sulfate (Na_2SO_4). The solvent was removed under reduced pressure and the residue was separated by column chromatography (silica gel, 2:1 v/v, petroleum ether/ dichloromethane). Yield: 2.6 g of yellow powder (90%). ^{1}H NMR (400 MHz, $CDCl_3$): δ 8.28 (dd, J = 8.2, 7.5 Hz, 1H), 8.07 (d, J = 7.7 Hz, 2H), 8.03–7.89 (m, 4H), 7.45 (d, J = 7.8 Hz, 4H), 7.34 (m, J = 7.3, 1.5 Hz, 8H). ^{13}C NMR (100 MHz, $CDCl_3$): δ 166.4, 153.8, 139.3, 138.6, 127.0, 126.6, 126.0, 124.1, 119.9, 116.0. HRMS (ESI): *m/z* calcd. for $C_{31}H_{20}N_3O_2$ $[M+H]^+$, 466.1550; found, 466.1547.

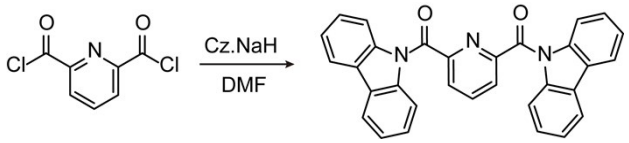

Scheme S1. Synthetic route of **DCzCOPy**.

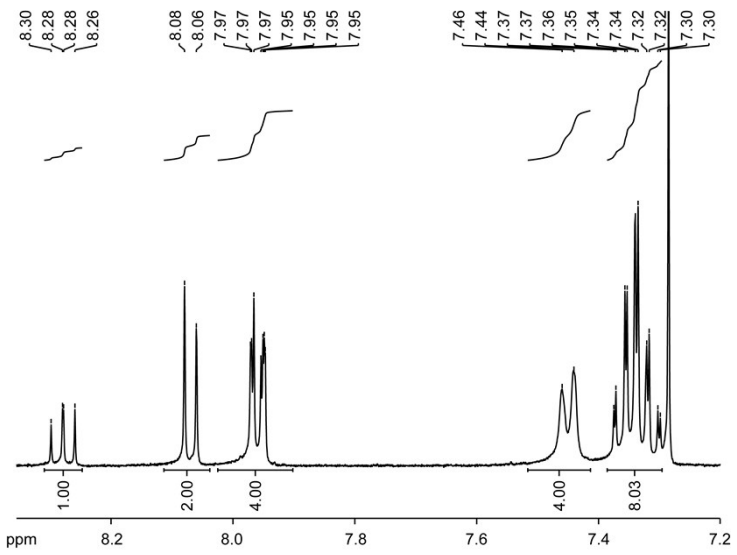

Figure S1. ^{1}H NMR spectrum of **DCzCOPy** in $CDCl_3$.

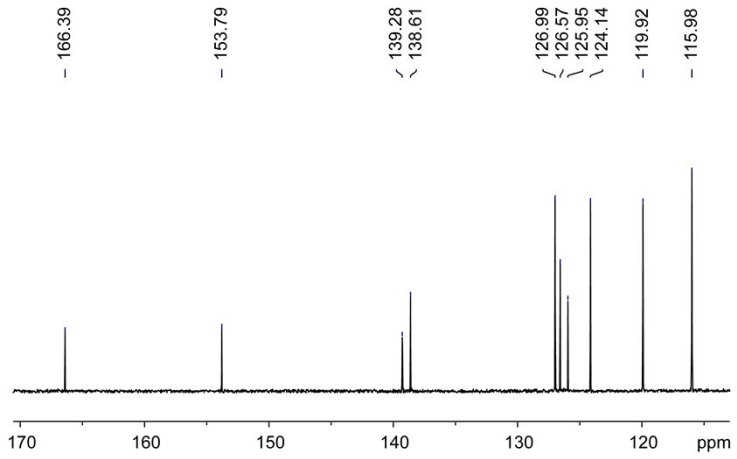

Figure S2. ^{13}C NMR spectrum of **DCzCOPy** in $CDCl_3$.

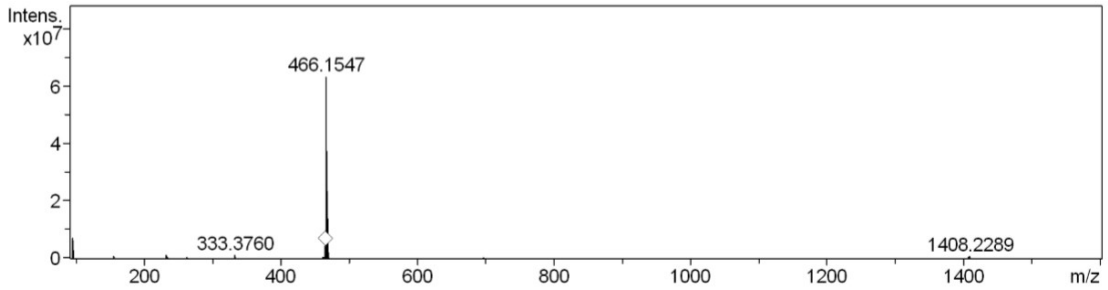

Figure S3. HRMS of **DCzCOPy**.

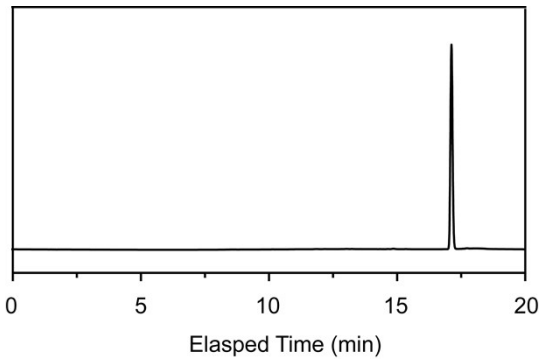

Figure S4. HPLC spectrum of **DCzCOPy** monitored at the onset absorption of 346 nm with 50/50 acetonitrile (ACN)-water ratio (v/v).

(9*H*-carbazol-9-yl)(phenyl)methanone (CPM)

CPM was synthesized according to the literature.[1] Into a 50 mL flask were placed with NaH (0.34 g, 9.9 mmol). Then, carbazole (0.835 g, 5 mmol) in DMF (20 mL) was added dropwise with stirring. After half an hour, a solution of 4-methylbenzoyl chloride (1 mL, 7.5 mmol) in DMF (10 mL) was added dropwise. The reaction mixture was stirred overnight. After quenched with water, the mixture was extracted with CH_2Cl_2 (3×40 mL). The combined organic layer was washed with water for several times to remove DMF, dried over anhydrous Na_2SO_4, and then concentrated by evaporation under reduced pressure. The residue was separated by column chromatography (silica gel, 20:1 v/v, petroleum ether/ ethyl acetate). Yield: 0.88 g of yellow powder (~64%). ^{1}H NMR (400 MHz, DMSO) δ 8.26 – 8.19 (m, 2H), 7.78 – 7.70 (m, 3H), 7.65 – 7.58 (m, 2H), 7.44 – 7.35 (m, 6H). ^{13}C NMR (100 MHz, DMSO) δ 169.1, 138.5, 135.4, 132.5, 129.1, 128.6, 126.9, 125.4, 123.5, 120.4, 115.3.

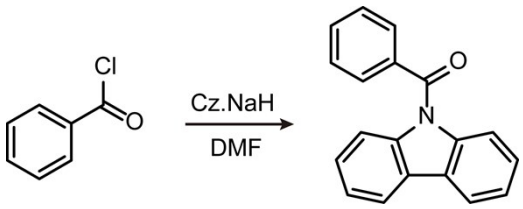

Scheme S2. Synthetic route of **CPM**.

1,3-phenylenebis((9*H*-carbazol-9-yl)methanone) (DCzCOPh)

DCzCOPh was synthesized according to the literature.[2] Into a 50 mL two necked round-bottom flask were placed with NaH (0.239 g, 5.98 mmol). Then, carbazole (0.50 g, 2.99 mmol) in

DMF (20 mL) was added dropwise with stirring. After half an hour, a solution of isophthaloyl dichloride (0.91 g, 4.49 mmol) in DMF (10 mL) was added dropwise. The reaction mixture was stirred overnight. After quenched with water, the mixture was extracted with CH_2Cl_2 (3×40 mL). The combined organic layer was washed with water for several times to remove DMF, dried over anhydrous Na_2SO_4, and then concentrated by evaporation under reduced pressure. The residue was separated by column chromatography (silica gel, 5:1 v/v, petroleum ether/ dichloromethane). Yield: 0.25 g of yellow powder (~35%).^{1}H NMR (400 MHz, $CDCl_3$): δ 8.15 (td, J = 1.8, 0.6 Hz, 1H), 8.06 – 7.96 (m, 6H), 7.72 (ddd, J = 8.0, 7.4, 0.6 Hz, 1H), 7.65 – 7.56 (m, 4H), 7.42 – 7.35 (m, 8H). ^{13}C NMR (100 MHz, $CDCl_3$) δ 168.1, 138.9, 136.9, 132.5, 129.6, 129.5, 126.9, 126.2, 123.8, 120.0, 115.8.

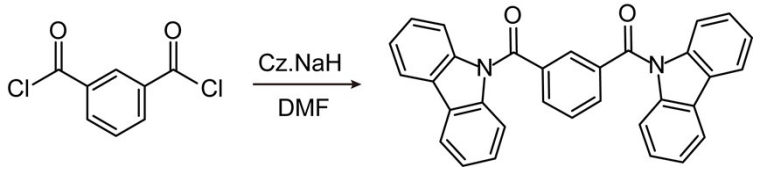

Scheme S3. Synthetic route of **DCzCOPh**.

2. Thermal properties

Thermogravimetric analysis (TGA) was conducted on a DTG-60 Shimadzu thermal analyst system under a heating rate of 10ºC/min and a nitrogen flow rate of 50 cm^3/min. The differential scanning calorimetry (DSC) analysis was performed on a Shimadzu DSC-60A instrument under a heating rate of 10ºC/min and a nitrogen flow rate of 20 cm^3/min.[3]

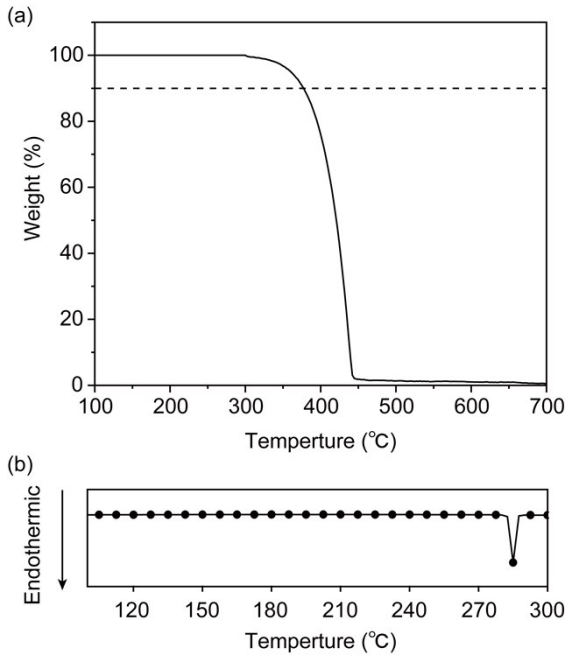

Figure S5. TGA (a) and DSC (b) curves of **DCzCOPy**.

3. Photophysical investigations

Ultraviolet/visible (UV/Vis) absorption and photoluminescence (PL) spectra were recorded on a Jasco V-750 spectrophotometer and Edinburgh FLS980 spectrophotometer, respectively. The absolute photoluminescence quantum yield (PLQY) was obtained using an Edinburgh FLS980 fluorescence spectrophotometer equipped with an integrating sphere. The phosphorescence quantum yield was calculated by the peak fitting method that had been widely used in recent publications.[4, 5] For fluorescence decay measurements, a picosecond pulsed light-emitting diode (EPLED-380, wavelength: 377 nm; pulse width: 947.7 ps) was used. Phosphorescence spectra were obtained using an Edinburgh FLS980 fluorescence spectrophotometer at 77 K with a 10 ms delay time after excitation using a microsecond flash lamp. The microsecond flash lamp produces short, typically a few μs, and high irradiance optical pulses for phosphorescence decay measurements in the range from microseconds to seconds. The UV excited kinetic measurements, OURTP spectra and ultralong lifetime were also measured on an Edinburgh FLS980 fluorescence spectrophotometer. X-ray activated radioluminescence spectra and kinetic measurements were obtained by an Edinburgh FS5 fluorescence spectrophotometer equipped with a miniature X-ray source (AMPEK, Inc.). The X-ray excited afterglow lifetime was measured by kinetic measurement using an Edinburgh FS5 fluorescence spectrophotometer. The lifetimes (τ) of the luminescence were obtained by fitting the decay curve with a multi-exponential decay function of [6]

$$I(\mathrm{t}) = \sum_i A_i e^{-\frac{t}{\tau_i}}$$

where A_i and τ_i represent the amplitudes and lifetimes of the individual components for multi-exponential decay profiles, respectively.

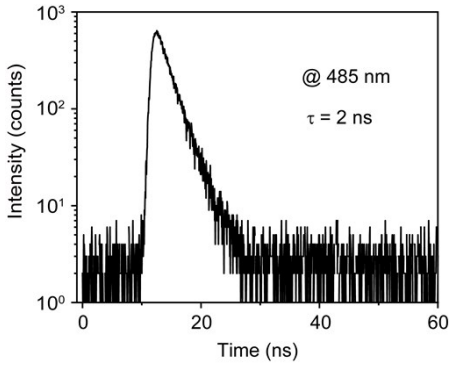

Figure S6. Fluorescence (485 nm) decay profile of **CzPAB** powder at 300 K. The excitation

wavelength is 395 nm.

To systemically investigate the influence of excitation intensity and duration on the OURTP properties, kinetic analyses were performed. The excitation intensity is regulated by tuning the Iris aperture of Edinburgh FLS980 from 20% to 100%. In **Figures S6a, b**, the excitation light at 395 nm with varied Iris was turned on and maintained for 10 s, and then turned off. Both of steady-state and OURTP emission were strengthened with the increasing of excitation intensity. Notably, the OURTP emission remains stable during the excitation and then decay exponentially after turned-off the excitation light, demonstrating also its ultralong lifetime feature. In **Figures S6c, d**, the influence of excitation duration on the OURTP emission was studied by measuring its intensity through varying irradiation duration time. The steady-state and OURTP emission intensities increase rapidly and become almost constant when the excitation duration varies from 1 to 10 s. These results indicate that the OURTP emission can be effectively motivated by low intensity and short duration of incident UV light under ambient conditions.

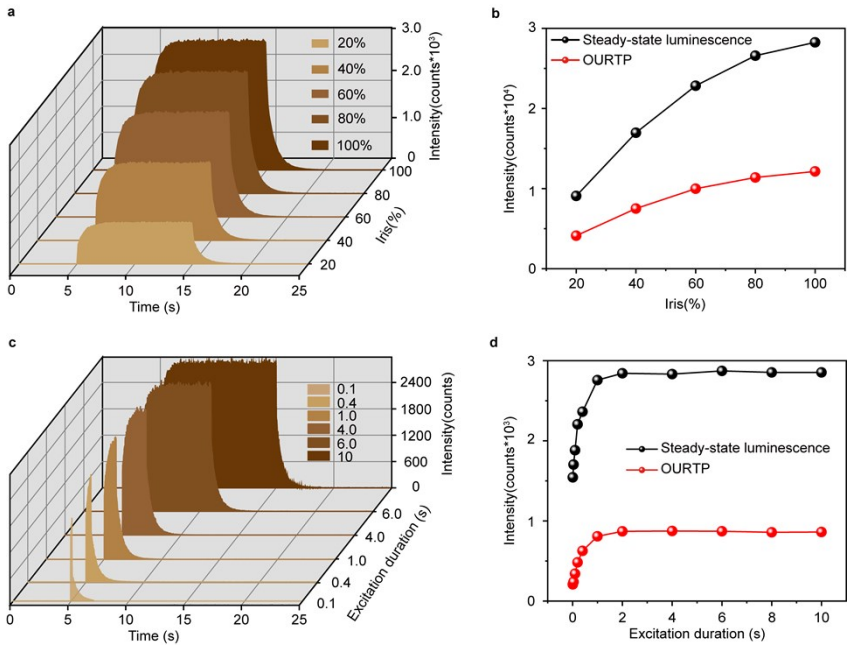

Figure S7. (a) Photoluminescence (PL) intensity profiles of 531 nm emission of **DCzCOPy** powder. (b) Steady-state PL (black) and OURTP (red) intensities at 531 nm as a function of time and Iris (20, 40, 60, 80 and 100%) excited at 395 nm under ambient conditions. (c) PL intensity profiles of 531 nm emission of **DCzCOPy** powder with (d) corresponding steady-state PL (black) and OURTP (red) intensities as a function of time upon 395 nm excitation with different irradiating durations (0.1, 0.4, 1.0, 4.0, 6.0, and 10 s) under ambient conditions.

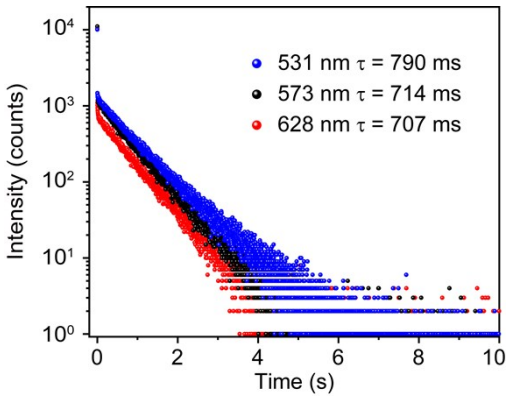

Figure S8. OURTP decay profiles of **DCzCOPy** powder at 300 K. The excitation wavelength is 395 nm.

Table S1. OURTP lifetimes of **DCzCOPy** crystal excited by 395 nm UV-light under ambient conditions

λ_{em} (nm)	τ_1 (ms)	A_1 (%)	χ^2
531	790	100	1.175
573	714	100	1.244
628	707	100	1.105

DCzCOPy crystals demonstrate almost identical afterglow spectra and decay profiles in air, argon (Ar) and oxygen (O_2) (**Figure S9**), suggesting the existence of dense molecular arrangement to prevent the depletion of the excited triplet excitons through blocking the oxygen penetration from the surrounding environment and suppressing the molecular vibration.

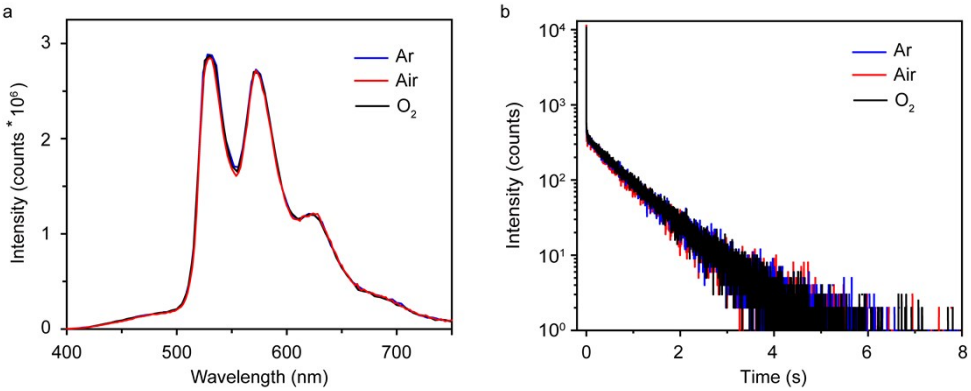

Figure S9. Organic afterglow spectra (a) and decay profiles (b) of **DCzCOPy** crystals excited by 365 nm in different atmospheres of Ar, air and O_2 at room temperature.

4. Theoretical calculation

Density functional theory (DFT) and time-dependent DFT (TD-DFT) calculations were performed using Gaussian 09 package with the Becke's three-parameter exchange functional along with the Lee Yang Parr's correlation functional (B3LYP) using 6-31G (d) basis sets. Dalton program with quadratic response function method was used to predict spin-orbit coupling (SOC) matrix elements between the lowest singlet excited state (S_1) and T_1. [7,8] Natural transition orbital (NTO) analysis was performed to get insights into the whole picture of the excited states with a compact orbital representation for the electronic transition density matrix. Charge difference density (CDD) upon the $S_1 \rightarrow S_0$ transitions based on the optimized single molecule and dimer structure extracted from the single-crystal were carried out using Multiwfn by subtracting the charge density of the grounded-state (S_0) from that of interested singlet excited state. The blue and green colors correspond to the decrease and increase of the charge density, respectively. The orbital delocalization index was calculated based on the orbital composition analysis of Multiwfn. [9]

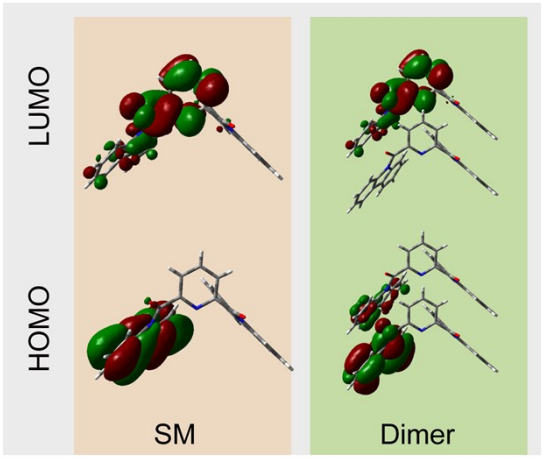

Figure S10. HOMO and LUMO isosurfaces of single molecular (SM) and dimer states.

Table S2. TD-DFT predicted singlet and triplet excited state energies and transition configurations of **DCzCOPy**.

Excited state	***n*-th**	**Energy (eV)**	**Transition configuration (%)**
S_n	1	3.5129	H→L (98.47)
T_n	1	3.1174	H-1→L(80.91), H-1→L+5(2.63), H→L(5.14)
	2	3.1932	H-8→132(2.62), H-1→L(5.44), H-1→L+7(6.55), H→L(21.99), H→L+1(3.3), H→L+2(3.61), H→L+3(16.45), H→L+4(30.49)
	3	3.2117	H-9→L+8(3.09), H-6→L+3(2.89), H-3→L+1(4.21), H-3→L+2(13.31), H-3→L+5(2.02), H-3→L+6(3.41), H-2→L+1(13.81), H-2→L+2(45.59)
	4	3.501	H-7→L(3.02), H-5→L(7.13), H-1→L(2.34), H→L(54.35), H→L+3(5.39), H→L+4(11.81)
	5	3.5395	H-12→L(2.14), H-10→L(4.38), H-7→L(15.17), H-6→L(6.58), H-5→L(29.77), H-5→L+1(3.73), H-4→L(5.42), H→L(14.79)
	6	3.6884	H-9→L+2(2.99), H-6→L+5(3.91), H-6→L+6(4.23), H-3→L(19.06), H-3→L+2(9.39), H-3→L+3(20.62), H-3→L+4(6.46), H-2→L(6.22), H-2→L+2(3.26), H-2→L+3(9.19), H-2→L+4(2.75), H-2→L+8(2.13)
	7	3.7943	H-3→L(2.98), H-3→L+1(30.98), H-3→L+2(29.38), H-3→L+3(3.31), H-3→L+4(2.08), H-2→L+1(11.15), H-2→L+2(8.23), H-2→L+3(2.25)
	8	3.816	H-4→L+7(4.54), H-1→L+1(7.58), H-1→L+2(4.81), H-1→L+3(21.18), H-1→L+4(43.52), H-1→L+5(2.16)
	9	3.8477	H-11→L(7.01), H-11→L+1(3.05), H-10→L(9.45), H-10→L+1(2.29), H-7→L(45.54), H-7→L+1(2.25), H-6→L(2.1), H-4→L(4.81), H-2→L(2.68)
	10	3.8939	H-3→L+3(2.92), H-2→L(83.99)

Table S3. TD-DFT calculated excited state energies and the spin-orbit coupling (SOC) constants between S_1 and T_n of **DCzCOPy**.

S_1/T_n	S_1/T_n energy gap	SOC
S_1/T_1	0.3955	0.82
S_1/T_2	0.3197	1.46
S_1/T_3	0.3012	0.21
S_1/T_4	0.0119	1.29
S_1/T_5	-0.0266	0.51
S_1/T_6	-0.1755	0.10
S_1/T_7	-0.2814	0.14
S_1/T_8	-0.3031	0.08
S_1/T_9	-0.3348	0.60
S_1/T_{10}	-0.381	0.13

5. Charge transfer feature

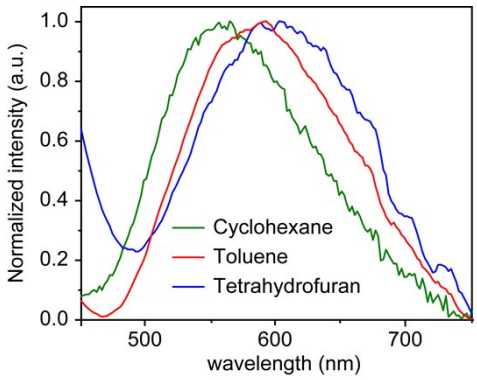

Figure S11. PL spectra of **DCzCOPy** in different solvents of cyclohexane, toluene, and tetrahydrofuran with increasing polarities at room temperature (~ 10^{-5} mol L^{-1}).

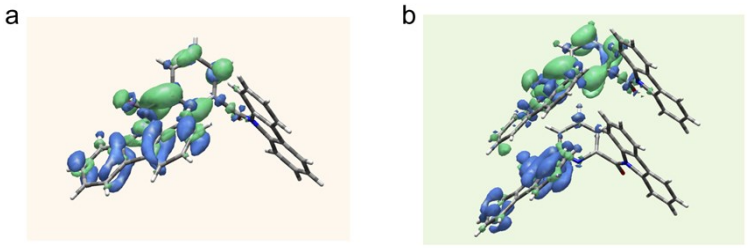

Figure S12. CDD plots upon $S_1 \rightarrow S_0$ transitions at single molecule (a) and dimer (b) states of **DCzCOPy**.

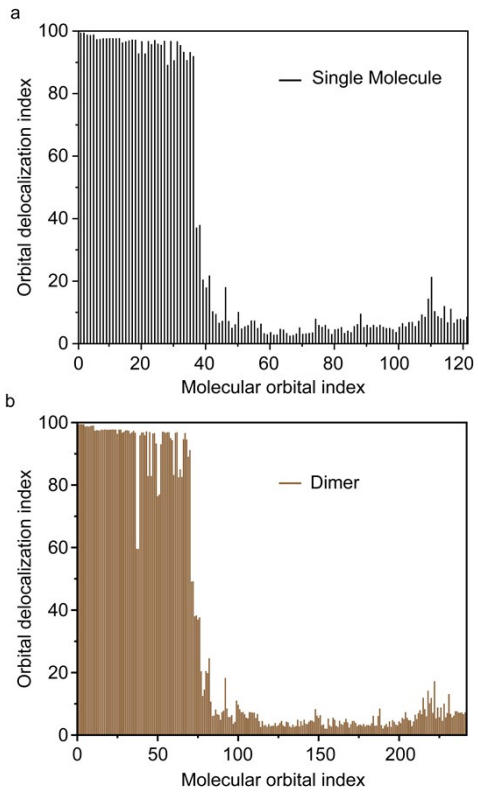

Figure S13. Orbital delocalization index (ODI) at single molecule (a) and dimer (b) structures of **DCzCOPy**.

6. Radioluminescence investigation of X-OURTP

To prove the proposed mechanism of X-OURTP, the radioluminescence investigations of carbazole (**Cz**) and **CPM** crystals (part of the **DCzCOPy**) and **DCzCOPh** crystals were performed. Compared to **DCzCOPy** crystal, **Cz** and **CPM** crystals exhibited almost neglected radioluminescence (**Figure S14a**), suggesting that the efficient charger transfer is of central importance to boost high π-electron mobility for the facilitated scintillation process. To further reveal the vital role of pyridine in achieving efficient scintillation property, we prepared another control molecule of **DCzCOPh** by the replacement of central pyridine with benzene. **DCzCOPh** crystals showed quite weak radioluminescence in comparison to that of **DCzCOPy** crystals. The enhanced RL emission of **DCzCOPy** should be due to its strong CT nature induced by the strong electron-withdrawing ability of the central pyridine for enhanced π-electron mobility. The reinforced CT property of **DCzCOPy** can be theoretically confirmed by the CT amount (*q*) simulation showing high *q* value compared to that of **DCzCOPh** (**Figure S14b**).

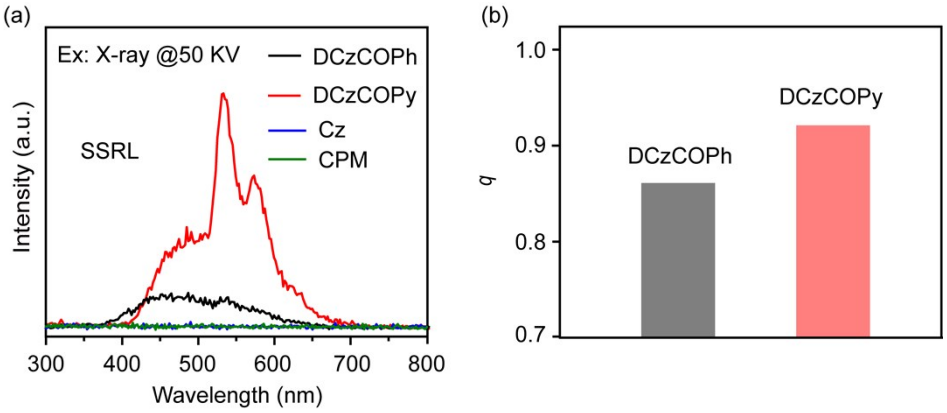

Figure S14. (a) Steady-state radioluminescence (SSRL) of **Cz**, **CPM, DCzCOPy** and **DCzCOPh** crystals under X-ray irradiation. (b) CT amount (q) of **DCzCOPy** and **DCzCOPh** of the single molecule at S_0 state.

7. Single crystals analyses

Single crystal of **DCzCOPy** was obtained by slow evaporation of a mixed DCM and petroleum ether solution at room temperature. The single crystal structure XRD data were collected on a Bruker SMART APEX (II)-CCD at 296K and crystal structure was analyzed by Mercury 1.4 software. Single crystal data were summarized in **Table S4**.

Table S4. Crystallographic data of **DCzCOPy**.

Empirical formula	**$C_{31}H_{19}N_3O_2$**
Formula weight (g mol^{-1})	465.49
Crystal color	yellow
Wavelength (Å)	0.71073
Crystal system	Triclinic
Space group	P-1
a, (Å)	5.1443(6)
b, (Å)	14.4148(3)
c, (Å)	14.9692(5)
α, (deg)	92.880
β, (deg)	93.257
γ, (deg)	90.232
volume, ($Å^3$)	2167(4)
Z	2
Density, (g cm^{-3})	1.397
μ, (mm^{-1})	0.089
F(000)	484
h_{max}, k_{max}, l_{max}	6, 18, 19
$Theta_{max}$	27.878
CCDC	2006857

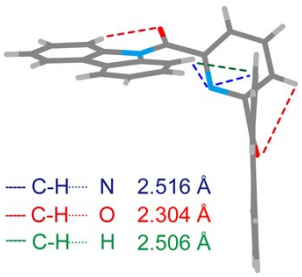

Figure S15. Intramolecular interactions in single crystal of **DCzCOPy**.

Aggregation structures have great influence on the photophysical properties of organic optoelectronic materials. Particularly, H-aggregation plays a vital role in stabilizing the excited triplet excitons for achieving the OURTP emission at solid states. The presence of H-aggregation can be verified by Frenkel exciton theory based on the single crystal structure, where the exciton splitting energy (Δε) of the selected dimer can be simulated by: [10, 11]

$$\Delta\varepsilon = \frac{2|M|^2}{r_{uv}^3}\left(\cos\alpha - 3\cos\theta_1\cos\theta_2\right)$$

where M is the transition moment that can be simulated by TD-DFT computation, r_{uv} is the intermolecular distance between the selected dimer, α is the angle between the transition dipole moments, θ_1 and θ_2 are angles between transition dipole moments of the two molecules and the interconnection of their molecular centers. When $\Delta\varepsilon>0$, it is H-aggregation, and when $\Delta\varepsilon<0$, it belongs to J-aggregation.

Table S5. H-aggregates in **DCzCOPy** crystals identified by the positive $\Delta\varepsilon$.

H-aggregate	α (°)	θ_1 (°)	θ_2 (°)	M (Debye)	r_{uv} (Å)	Δε (eV)
H1	180.0	150.6	29.4	0.29	13.75	0.000052
H2	180.0	137.7	42.3	0.29	11.78	0.000041
H3	180.0	132.7	47.3	0.29	11.38	0.000027
H4	180.0	54.6	125.4	0.29	9.82	0.000001
H5	180.0	47.9	132.1	0.29	10.00	0.000037
H6	180.0	43.6	136.4	0.29	12.36	0.000032
H7	180.0	34.9	145.1	0.29	12.15	0.000060

7. References

[1] S. Cai, H. Shi, J. Li, L. Gu, Y. Ni, Z. Cheng, S. Wang, W. Xiong, L. Li, Z. An, W. Huang, *Adv. Mater.*, **2017**, *29*, 1701244.

[2] Z. He, H. Gao, S. Zhang, S. Zheng, Y. Wang, Z. Zhao, D. Ding, B. Yang, Y. Zhang, W. Z. Yuan, *Adv. Mater*., **2019**, *31*, 1807222.

[3] W. Zhao, T. S. Cheung, N. Jiang, W. Huang, J. W. Y. Lam, X. Zhang, Z. He and B. Z. Tang, *Nat. Commun.*, **2019**, 10, 1595.

[4] J. Jin, H. Jiang, Q. Yang, L. Tang, Y. Tao, Y. Li, R. Chen, C. Zheng, Q. Fan, K. Y. Zhang, Q. Zhao, W. Huang, *Nat. Commun*., **2020**, *11*, 842.

[6] Y. Tao, R. Chen, H. Li, J. Yuan, Y. Wan, H. Jiang, C. Chen, Y. Si, C. Zheng, B. Yang, G. Xing, W. Huang, *Adv. Mater*., **2018**, *30*, 1803856.

[6] H. Li, H. Li, W. Wang, Y. Tao, S. Wang, Q. Yang, Y. Jiang, C. Zheng, W. Huang, R. Chen, *Angew Chem. Int. Ed.,* **2020**, *59*, 4756-4762.

[7] K. Aidas, C. Angeli, K. L. Bak, V. Bakken, R. Bast, L. Boman, O. Christiansen, R. Cimiraglia, S. Coriani, P. Dahle, E. K. Dalskov, U. Ekstrom, T. Enevoldsen, J. J. Eriksen, P. Ettenhuber, B. Fernandez, L. Ferrighi, H. Fliegl, L. Frediani, K. Hald, A. Halkier, C. Hattig, H. Heiberg, T. Helgaker, A. C. Hennum, H. Hettema, E. Hjertenaes, S. Host, I. M. Hoyvik, M. F. Iozzi, B. Jansik, H. J. Jensen, D. Jonsson, P. Jorgensen, J. Kauczor, S. Kirpekar, T. Kjaergaard, W. Klopper, S. Knecht, R. Kobayashi, H. Koch, J. Kongsted, A. Krapp, K. Kristensen, A. Ligabue, O. B. Lutnaes, J. I. Melo, K. V. Mikkelsen, R. H. Myhre, C. Neiss, C. B. Nielsen, P. Norman, J. Olsen, J. M. Olsen, A. Osted, M. J. Packer, F. Pawlowski, T. B. Pedersen, P. F. Provasi, S. Reine, Z. Rinkevicius, T. A. Ruden, K. Ruud, V. V. Rybkin, P. Salek, C. C. Samson, A. S. de Meras, T. Saue, S. P. Sauer, B. Schimmelpfennig, K. Sneskov, A. H. Steindal, K. O. Sylvester-Hvid, P. R. Taylor, A. M. Teale, E. I. Tellgren, D. P. Tew, A. J. Thorvaldsen, L. Thogersen, O. Vahtras, M. A. Watson, D. J. Wilson, M. Ziolkowski, H. Agren, *WIREs Comput. Mol. Sci*., **2014**, *4*, 269-284.

[8] J. Yuan, R. Chen, X. Tang, Y. Tao, S. Xu, L. Jin, C. Chen, X. Zhou, C. Zheng, W. Huang, *Chem. Sci*., **2019**, *10*, 5031-5038.

[9] T. Lu, F. Chen, *J. Comput. Chem*., **2012**, 33, 580-592.

[10] M. Kasha, H. R. Rawls, M. Ashraf El-Bayoumi, *Pure Appl. Chem*., **1965**, 11, 371.

[11] Z. An, C. Zheng, Y. Tao, R. Chen, H. Shi, T. Chen, Z. Wang, H. Li, R. Deng, X. Liu, W. Huang, *Nat. Mater*., **2015**, *14*, 685-690.